Clay Minerals (2025), 1–10
doi:10.1180/clm.2025.10009

Article

Climatic and tectonic influences as recorded in the mineralogy of a Miocene clay deposit at Şile, Türkiye

Orhan Yavuz[1], Paul A. Schroeder[2], Huseyin Demir[3] and Ö. Isik Ece[1,2]

[1]İstanbul Technical University, Geological Engineering, Faculty of Mines, Maslak, İstanbul, Türkiye; [2]Department of Geology, University of Georgia, Athens, GA, USA and [3]General Directorate of State Hydraulic Works: DSI Genel Mudurlugu, Ankara, Türkiye

Abstract

Miocene lacustrine clay deposits formed in the Şile region of Türkiye rest unconformably on Cretaceous andesite, basaltic andesite, basalts and rare dacites. Factors controlling the genesis of this sequence include: (1) sediment provenance, (2) tectonic uplift and climatic regimes during syn- and post-depositional times, (3) burial diagenesis and (4) changes from surface weathering alterations (i.e. oxidation and hydrolysis reactions) in the critical zone. Clay minerals are dominated by kaolinite and illite, with their relative abundances varying in relation to the proximity of coal seams, stratigraphic sequence and in an overlying sand-rich fluvial deposit. Variations in the mineral abundances reveals cyclothem-like sequences with patterns of fining upwards (i.e. increasing clay mineral abundance) capped by thin coal seams. The Clay Mineral Alteration Index values for the Şile clay sequence indicate a slight trend of decreasing chemical weathering intensity up-section, which is consistent with regional geological data for terrain uplifting and a drying climate during the Miocene. Critical zone processes have modified the mineral and chemical assemblages, as evidenced by the appearance of iron oxides putatively formed from recent oxidation of the ferrous minerals siderite and pyrite, which are not found in the upper sections. Taken together, the evidence indicates that the clay minerals are derived from a combination of prior weathering of basement rocks, diagenesis after deposition and modern critical-zone weathering. The degree of each process is dependent on depositional history, stratigraphic position and depth below the land surface, all under the changing influences of tectonic uplift and regional climate. The Şile deposits provide an economical clay resource that could be important to the ceramics industry of Türkiye.

Keywords: Clay deposits; clay fraction geochemistry; clays; critical zone; kaolinite; palaeo-environment; provenance; X-ray diffraction

(Received 18 December 2024; revised 19 June 2025; Manuscript Accepted online: 24 June 2025; Associate Editor: F. Javier Huertas)

The Şile kaolin deposits represent some of Türkiye's largest natural resources and hold significant economic importance (Ece *et al.*, 2003). Globally, kaolinite has extensive industrial applications, including its use in ceramics, paints, paper, pharmaceutical products, cement, membranes, geopolymers, wastewater treatment, catalysis, pesticides, detergents and cosmetics (Murray & Keller, 1993; Awwad *et al.*, 2020; Gianni *et al.*, 2020; Zhang *et al.*, 2020; Zunino *et al.*, 2020; Cao *et al.*, 2021; Fellah *et al.*, 2021; Mubarak *et al.*, 2021; Olu-Owolabi *et al.*, 2021; Rashad *et al.*, 2023).

Beyond its industrial applications, these kaolinite-rich deposits also serve as mineralogical markers, preserving palaeo-environmental information that can aid in reconstructing the geological history of a region. Kaolinite-bearing units can carry signals and indicators of climatic weathering processes, parent material alteration and soil development mechanisms across both spatial and temporal scales – on Earth and other planets (Fackrell *et al.*, 2020; Warr, 2022). The goal of this study is to examine the vertical mineralogical and chemical variations within a well-exposed kaolin mining site, with the aim of understanding the factors that influence the suitability of these minerals as proxies for environmental change. These observations provide a framework for future studies focused on spatial and temporal changes in mineralogy, with the broader objective of understanding sediment provenance and the geological evolution of the Şile region, particularly during the Miocene, when they were deposited.

The mineral and chemical composition of any given layer within the deposit is assumed to be controlled by three primary geological factors: (1) the sediment provenance and environmental conditions at the time of deposition; (2) burial diagenetic alteration following deposition; and (3) meteoric weathering upon exposure, driven by tectonics and climate change. These factors are increasingly viewed within the broader framework of critical-zone (CZ) science, which examines the physical, chemical and biological alteration of regolith, encompassing processes from the treetops to the bedrock (Schroeder, 2018; Richter *et al.*, 2020). We posit that, in addition to the first two factors being key determinants of ore quality and industrial application, more recent CZ processes may also represent significant modifiers of the mineralogical and chemical

Corresponding author: Paul A. Schroeder; Email: schroe@uga.edu

Cite this article: Yavuz O, Schroeder PA, Demir H and Ece ÖI (2025) Climatic and tectonic influences as recorded in the mineralogy of a Miocene clay deposit at Şile, Türkiye. *Clay Minerals*, 1–10. https://doi.org/10.1180/clm.2025.10009

properties of these deposits. We hypothesize that the mineral and chemical properties of this lacustrine deposit have recorded a trend of oscillatory climatic and region changes indicating an overall pattern of drying and uplift. This study updates the work of Ece *et al.* (2003) by adding a more quantitative assessment of the mineralogy and chemistry and further consideration of modern CZ weathering processes as factors influencing the abundances and types of clays in the Şile deposits.

Geological background of Şile clays

The surrounding basement rocks in the Şile region include the İstanbul Palaeozoic sedimentary sequence, Permian–Triassic sedimentary rocks, Lower Cretaceous flysch series and Upper Cretaceous volcanic rocks and their equivalent of volcanoclastics (Fig. S1). Collectively, the rocks comprise the İstanbul zone, which is interpreted as a rifted fragment from the Odessa shelf that was translated to the south with the opening of the western Black Sea basin (Okay & Kelley, 1994). The İstanbul Palaeozoic sequence known as the Istanbul zone is characterized by a well-developed, unmetamorphosed and little-deformed continuous Palaeozoic sedimentary succession extending from the Lower Ordovician to the Lower Carboniferous overlain with a major unconformity by latest Permian to lowermost Triassic continental red beds (Okay, 1989). This sedimentary sequence is represented by different regressive and transgressive basin units, which were intensely faulted. The sequence starts with Lower Ordovician clastics composed of marine turbidites, deltaic deposits that passed upwards into terrestrial fluvial units composed of purple arkosic conglomerate, sandstone, siltstone and shale intercalations. These were overlain by Lower Ordovician shore–shallow-sea quartz sandstones and lagoonal–shelf facies then followed by Middle Ordovician to Lower Silurian conglomerates and shale and sandstone–shale. These formations were overlain by Upper Silurian to Lower Devonian limestone, nodular limestone (shelf–deep shelf transition) and then limestone interlayered with micaceous shale and sandstone that were Early to Middle Devonian in age, deposited in a deep shelf facies. These were followed by Middle to Upper Devonian–early Carboniferous cherty limestone (deep shelf slope) and Lower to Middle Carboniferous turbiditic sandstone and shale alternation in the uppermost of the Palaeozoic succession (Gedik *et al.*, 2005). Various formation names have been used in different review studies for these Palaeozoic units. Recently, Özgül (2011, 2012) distinguished members of the İstanbul Palaeozoic zone in more detail. The İstanbul Palaeozoic sedimentary sequence was also summarized by Lom *et al.* (2016).

The Permian–Lower Triassic (Permo-Triassic, Early to Middle Triassic?) terrestrial successions unconformably cover the Palaeozoic units in the study area. These successions are divided into three partly different units (Gedik *et al.*, 2005). These start at the bottom with red-coloured fluvial deposits and pass into shallow-water sandstone and carbonate. Sandy and clayey limestone, dolomitic limestone and dolomites characterizing shallow shelves overlie these units (Yurtsever, 1982). These series were found only around thrust zones within the study area but are more common farther to the east. Upper Triassic and Jurassic rocks were absent from the study area.

The Cretaceous volcanic sequence sits on the Palaeozoic and Triassic units with angular unconformity. A volcanic and volcano-sedimentary unit is found in the northern part of the study area, which is related to arc magmatism resulting from the north-dipping subduction of the Neo-Tethys Ocean along the İzmir–Ankara–Erzincan suture (Şengör & Yılmaz, 1981). Yavuz & Yılmaz (2010) defined the mineralogical, petrographic and geological characterization of volcanites in the north of Istanbul. Using isotopic data from the Central Pontides, Okay *et al.* (2006) concluded that the Neo-Tethys was already subducting under the Pontides in the Early Cretaceous (~105 Ma), with the magmatic arc beginning to develop in the Late Cretaceous. However, the western Black Sea basin is believed to have opened during the Early Cretaceous as a back-arc basin above the northwards-subducting Tethys Ocean (Adamia *et al.*, 1974; Hsü *et al.*, 1977; Letouzey *et al.*, 1977; Görür, 1988, 1991, 1997; Manetti *et al.*, 1988). U-Pb zircons obtained from calc-alkaline andesitic to dacitic dikes within the İstanbul Palaeozoic unit in the south yield ages ranging from 72.49 ± 0.79 to 65.44 ± 0.93 Ma (Aysal *et al.*, 2018). The volcanism ceased by the end of the Late Cretaceous (Şengör & Kindap, 2019), and these volcanic and volcano-sedimentary rocks are overlain by Upper Cretaceous–Palaeocene pelagic limestone and marl (Ketin, 1955).

During the Eocene, multiple collisions of small continental fragments resulted in compressional movements, giving rise to pre-Lutetian folding and faulting in the study area (Şengör & Yılmaz, 1981; Gedik *et al.*, 2005). Palaeozoic and Mesozoic units were contemporaneously thrusted over the Upper Cretaceous–Lower Eocene sequences (Özgül, 2012), and this region is now known as the east–west striking Şile Thrust. The Şile Thrust is a back-thrust associated with the closing of the northern branch of the Neo-Tethys Ocean, known as the Intra-Pontide Ocean. The Lutetian shelf and shallow marine succession composed of interbedded shale–limestone and sandstone was deposited in the Şile region. Because of the movement of the Şile Thrust, the study area experienced rapid post-collisional uplift, and there was no deposition in the region until the Pliocene (Lom *et al.*, 2016). However, Gedik *et al.* (2005) suggested that deposition started in the Oligo-Miocene based on palynological data from the coal layer within the terrestrial clastic sediments. In places near the eastern and western İstanbul Bosphorus area (Sarıyer and Anadolu Kavağı), the Şile Thrust fault occurs as high-angle faults that include components of oblique transform and/or reverse faults as opposed to true thrust fault architecture.

All tectonic events leading up to the Miocene are herein collectively considered as the Palaeotectonic period. The new tectonic era (i.e. herein 'the Neotectonic') characterized the region since at least the Late Miocene. The elimination of the last portion of ocean between the Arabian and Anatolian plates developed the North Anatolian Shear System and gave rise to the North Anatolian Fault, which initiated its dextral strike-slip motion around the Late-medial Miocene (Ketin, 1966; Şengör *et al.*, 1985; Yılmaz, 1993; Le Pichon *et al.*, 2001; Okay *et al.*, 2008). Although the fault was initiated across the full region in the Pliocene (Bozkurt, 2001), the shear system has been extant since the Late Miocene (Şengör & Kindap, 2019) and reveals itself through extensional features in the area.

Analytical methods

The site location was influenced by the unique exposure offered by mining operations and public accessibility to key lithological outcrops. This suite enabled the highlighting of different chemical and mineral variations in the Şile region north-east of İstanbul and the testing of the hypothesis that such changes are proxies for geological and climatic shifts during the Miocene, as well as highlighting modifications due to recent exposure of the CZ. Samples included regional outcrops and a detailed section from a mine operated by

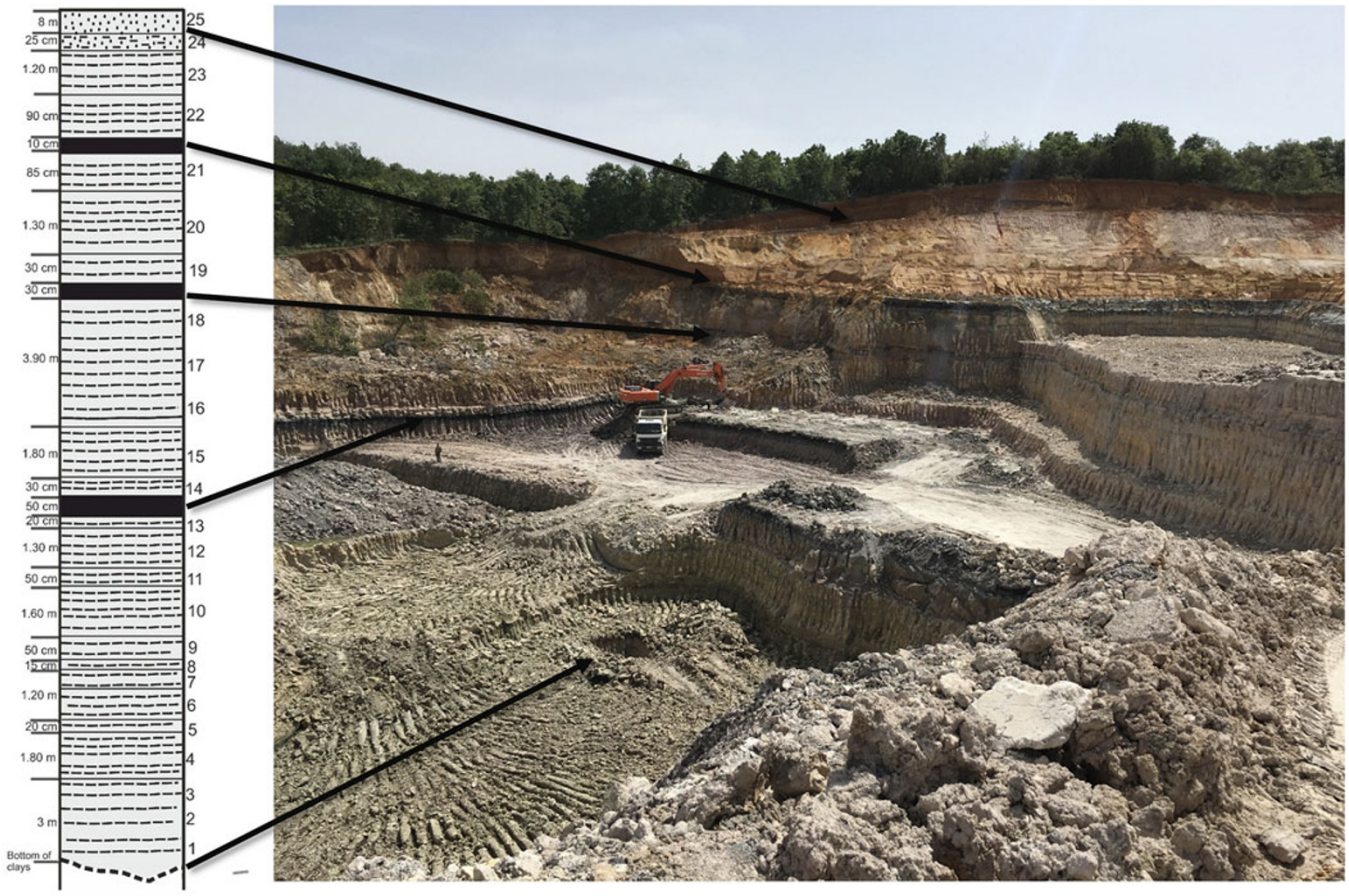

Figure 1. Photograph of mining operations on the day of sampling (operated by Erel Maden located at 41°8.619′N, 29°27.808′E). Sampling of representative layers was based on the lowest elevation of bench floors. Select and individual sample photos are shown in Figs S2 & S3. Sample positions and coal seams are shown in the schematic stratigraphic column to the left. Excavation equipment and operators are shown for scale.

Erel Maden (41°8.619′N, 29°27.808E; Fig. S1). The benched nature of the mine allowed for quasi-vertical sampling, with heights above the lowest excavation level recorded (Fig. S2). Twenty-five samples were collected in 2017, with general field descriptions given to each and measures taken of the sample section thickness (Fig. 1). The top three samples occurred in sand-rich facies cross-cut by a mud-filled dike interpreted as being a result of brittle fracturing and liquefaction mud emplacement during a tectonic event. Detailed photographs of all 2017 mine samples are presented in Fig. S3. The locations of basement outcrop samples and select quarry samples collected in 2019 are presented in Table S1.

X-ray powder diffraction (XRD) was used to characterize both bulk and clay fractions (<2 μm) in the mineral assemblages of the collected samples. Approximately 10 g of each sample was dried at 65°C overnight. Approximately 5 g of each dried sample was hand-ground with a corundum mortar. The powder was then further ground in a McCrone® micronizing mill for 10 min with 10 ml ethyl alcohol to reduce the particle size to an average of 5–10 μm. Ten percent by weight ZnO (zincite) was added as an internal standard (IS). Samples were dried to remove alcohol in an oven at 65°C overnight and then backfilled against plate glass into a 2.5 × 2.5 cm aluminium holder. The powder was pressed at 400 psi to make a flat self-supporting mount. This minimized sample transparency in the X-ray beam. A Bruker D8 Advance X-ray Diffractometer was configured using a 250 cm goniometer radius, a 0.6 mm divergent slit and Bragg–Bentano geometry. A knife-edge blade was placed 2 mm over the sample surface to minimize low-angle scatter into the Lynx-Eye® position-sensitive detector. A cobalt radiation source operated at 35 kV and 40 mA was used ($K\alpha_1 = 1.7890$ Å and $K\alpha_2 = 1.7928$ Å) with an iron filter to minimize $K\beta$ radiation. An external NIST Reference Standard SRM1976b corundum (α-Al_2O_3) was run to confirm alignment and calibration within 0.05°2θ tolerance of the certificate value for the strongest reflection peak position. The scan range extended from 2 to 80°2θ, using locked-coupled continuous scan mode with a step size of 0.01°2θ and a count rate of 0.1 s per step. Raw data and plots are presented with traces and peak positions determined by Bruker *Eva*® software. Raw data were $K\alpha_2$ stripped. The IS was used to correct for sample displacement error, which was usually less than 0.05°2θ. Peak positions were matched with data from the International Centre for Diffraction Data (ICDD) Powder Diffraction File (PDF) database. *Eva* software was used with the 2019-PDF database to find best-fit phases for mineral identification. Structure files for each phase identified were exported, which contained unit-cell lattice parameters, atom types and atomic coordinates. Many of the sample mineral assemblages included mixed-layer clay minerals. The ICDD-PDF does not contain structure files for mixed-layer clays; therefore, only discrete minerals could be assigned to bulk XRD traces.

Bruker *TOPAS*® software was used for semi-quantitative modelling of the samples. This program is based on the Rietveld refinement method (Rietveld, 1967). In brief, this method calculates the theoretical XRD trace for each phase using kinematic diffraction

theory (Schroeder, 2018). It then uses optimization schemes to minimize the difference between observed XRD data and calculated patterns. Included in the *TOPAS* software are options to optimize structure file data and other parameters such as preferred orientation crystal planes and mean coherent scattering domain size. The routine also optimizes total XRD intensity, which is related to abundance. In all cases, ZnO IS abundance was allowed to be optimized as a check for agreement between model results and the known weight fraction addition of the IS. In most cases, the agreement was within ±10% of the known amount added. Each refinement's goodness of fit was evaluated using the weighted profile *R*-factor (R_{wp}), which is fully explained by Toby (2006). Generally, model solutions with $R_{wp} < 15$ are considered acceptable for semi-quantitative analysis. It is important to note that the *TOPAS* software does not allow for mixed-layer structures to be included in the calculations; therefore, regardless of other optimization efforts, in some cases, satisfactory R_{wp} values were not achieved. Despite this limitation, consistent practices were used to keep model parameters with similar ranges of values to allow inter-sample comparisons of relative abundances.

For the fine fraction (<2 μm), ~10 g of each sample was taken and dried in an oven at 65°C overnight. The dried sample was placed in a centrifuge tube with a solution of 38 g of Na-hexametaphosphate and 8 g of Na-carbonate per litre of deionized water and dispersed using a Branson Sonifier Cell Disruptor 350 for ~1 min. The sample was then sieved to remove the sand fraction (>63 μm) with a 230 mesh sieve. The <2 μm clay fraction was separated from the <63 μm fraction using standard centrifugation techniques (Schroeder, 2018). The resultant slurry was considered Na-saturated after this treatment. This step was repeated for Ca-saturation by exchanging with 0.1 M $CaCl_2$ solutions. Deionized water was added to the slurry, and repeated centrifugation was applied again to remove excess salt (Austin *et al.*, 2020). This fine fraction was then dispersed in 25–30 mL of deionized water, drop-cast by pipette onto a glass petrographic slide (25 × 40 mm) and dried overnight. This drying process creates orientated particles that enhance the basal reflections of phyllosilicates/clay minerals. Select duplicate slides were prepared on select fresh samples for formamide intercalation testing to distinguish the presence of halloysite in kaolin-bearing samples (Churchman, 1990). For the formamide test, samples were exposed to formamide for ~30 min and then scanned.

The orientated slide(s) was scanned from 2 to 40°2θ using the locked-coupled continuous scan mode with a step size of 0.01°2θ and a count rate of 0.1 s per step. Data were collected for each sample in states of air-dried (AD) overnight at ambient relative humidity, ethylene glycolated (EG) overnight at 65°C in a closed EG atmosphere and heated in the oven overnight at 110°C, 350°C or 550°C. Based on the locations of the peaks and their movement, changes in intensity or disappearance depending upon stage of treatment, the types of clay minerals were identified. In the case of the orientated clay fractions, *NEWMOD2* software was used to determine the nature of the mixed-layer clay minerals for the EG-Ca-saturated state.

Inductively coupled plasma (ICP) optical emission spectroscopy (OES), mass spectrometry (MS) and loss on ignition (LOI) analyses were used to characterize the elemental compositions. Approximately 5 g of each sample were analysed by Activation Laboratories (Actlabs) in Ontario, Canada, for the 4-LITHO (with RX4 sample preparation) geochemical characterization of major oxides and trace elements. This method involves high-temperature (molten) lithium metaborate/tetraborate fusion performed by automation at Actlabs, and the resultant was immediately digested in a weak nitric acid solution. Analysis was performed through ICP-OES and ICP-MS (for detection limits, see https://actlabs.com). LOI was independently measured by heating a known sample mass to 950°C in an open atmosphere to volatilize carbonate, sulfates and hydroxide-bearing and organic matter components. Mass loss is measured after the heating treatment. Mass gain is possible if reduced iron is present, which reacts to form iron oxide.

Chemical data were recast as two different alteration indices. This first index was the Clay Mineral Alteration Index (CMAI) as defined by Warr (2022), where CMAI = (2:1 LE + 2:1:1 LE) – (1:1 LE + 2:1 HE) (numeric layer ratios are for tetrahedral:octahedral sheet combinations, LE = wt.% low expandable and HE = wt.% high expandable). CMAI values range from –100 to +100, acting as a proxy measure of the difference between physical weathering and newly formed clays. The second index was the Chemical Index of Alternation (CIA), where CIA = $(Al_2O_3/(Al_2O_3 + CaO + Na_2O + K_2O)) \times 100$ (Nesbitt & Young, 1982). The CMAI and CIA are related as measures of the intensity of chemical weathering history; however, they rely on different independent parameters, with the former based more on the abundances of clay products, whereas the latter is based on all primary minerals in an assemblage.

Results

Mineralogy and chemistry of the mine production site

A stratigraphic section of the quarry reveals deposits consisting of clay-rich, sand-rich and gravel-rich interbeds of various thicknesses (Fig. 1). The layers display a range of colours, including grey, yellowish-grey, greenish-grey, cream, pinkish- and reddish-brown, brown and blackish hues. These colours are primarily influenced by the relative amounts of organic material and iron-rich minerals. Sand- and gravel-rich lenses, as well as thick cyclic coal seams, were also observed. The uppermost part of the section features vertical reddish-brown clay dikes within the cream sand layer (Fig. S1). These deposits are associated with fluvial–lacustrine environments, as evidenced by channel lag gravels, small coal seams and the textures in the sand layers. The cyclic nature of the deposits, with alternating coarser and finer layers, suggests periodic changes in depositional conditions.

Whole-rock XRD analysis (Fig. 2 & Tables S2 & S3) shows that quartz and phyllosilicates dominate the mineral assemblages, with minor phases including anatase, gibbsite and goethite. Hematite, siderite and pyrite are present but not ubiquitous. The semi-quantitative Rietveld analysis results (Fig. 3) indicate that quartz, illite and kaolinite are the most abundant minerals, ranging from 15% to 50%, from 10% to 25% and from 20% to 60%, respectively.

The quartz abundance exhibits cyclical trends:

- From the base of the stratigraphic section upwards, quartz decreases from 50% to 10% at 6.35 m, then increases to 50% at 14.35 m.
- Quartz decreases again to 25% at 21.9 m, before sharply rising to 40% at 30 m at the top.

Kaolinite and illite abundance trends are antithetical to quartz, reflecting two fining-upward sequences followed by coarsening-upward sequences. Each cycle includes thin coal seams. While these cycles are not full cyclothems (*sensu stricto*, per Wanless & Weller, 1932), they are often reflective of an oscillatory climate

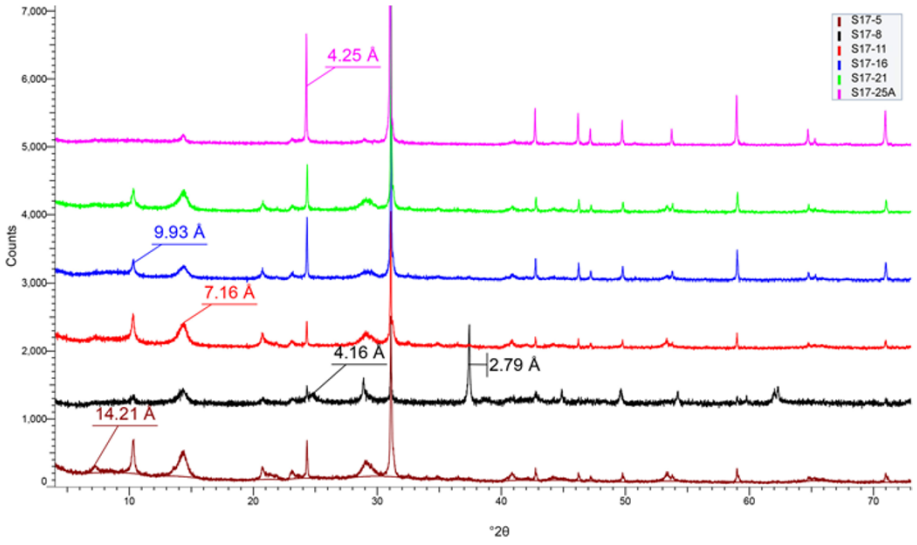

Figure 2. Representative bulk XRD traces showing major phases present in the stratigraphic section of the Erel Maden mine. Labels mark the location (*d*-spacing) of major minerals. Labelled peaks show illite (~9.93 Å), kaolinite (~7.16 Å), quartz (~4.25 and 3.33 Å), siderite (~3.58 and ~2.79 Å) and goethite (~4.16 Å). Data collected using Co-$K\alpha$ radiation.

and/or tectonic uplift. The CMAI values (Warr, 2022) for the Şile samples ranged from –70 to –92 (using bulk wt.% from the XRD analyses). Excluding the sandy cap section, there is a general trend of less negative CMAI values more upwards in the sequence, which is consistent with a change from 'newly formed' (i.e. chemical weathering-derived 1:1 and 2:1 expandable clays) to more detrital (i.e. physically weathered, low-expanding 2:1 and 2:1:1 clays) soil minerals upwards in the stratigraphic sequence (Warr, 2022). The CIA for the same suite of samples in the mine ranged from 85 to 96, thus indicating a history of intense weathering (Nesbitt & Young, 1982).

Analysis of the fine (<2 μm) fraction *via* XRD revealed kaolinite and illite as the dominant clay minerals (Fig. 4 & Table S2). Examination of orientated clay slides in various states (Ca-saturated, AD, EG and heated at 110°C, 350°C or 550°C) also identified minor amounts of interstratified chlorite/smectite, discrete chlorite, vermiculite, gibbsite and goethite. Tests for halloysite (formamide intercalation) were negative except in the three deepest samples, which showed slight formamide expansion of the 7 Å reflection. This is interpreted as minor 10 Å interstratified layering. The upper stratigraphic section samples contain more abundant interstratified ordered illite-smectite.

Mineralogy and chemistry of the basement rocks and caprock

Capping the quarry are sand-rich alluvial deposits (Fig. S2g). These sands are quartz-rich, and the clays predominantly consist of kaolinite (Fig. S4a,b). Near-vertical clay dikes cross-cutting the sand layers are dominated by kaolinite, chlorite, smectite and lesser amounts of illite. Poorly crystalline iron oxides and goethite occur as Liesegang-like bands, possibly formed by iron diffusion during wet/dry redox cycles. Alternatively, such self-organization of stripes has been explained by Dong *et al.* (2023) as resulting from redox fluctuations inducing nanoparticle dispersion and coagulation, termed 'turning patterns'. Given the more concentric pattern, we suggest that the mechanism of diffusion and precipitation (as opposed to reaction–diffusion with biological feedback) is the more likely formation process. These cycles may reflect geological timescale water table fluctuations, which is consistent with a trend towards an oscillatory drying climate and/or tectonic uplift.

The similarity of the clay mineral assemblages in the dikes and underlying quarry layers suggests clay injection during extensional movements caused by Neotectonic earthquakes (Fig. S2h). This is supported by the geometry of the dikes and their alignment with extensional stress patterns.

The basement rocks have very different clay mineral assemblages than the Miocene clay deposits. These include kaolinite, chlorite, interstratified chlorite-smectite and smectite. Late Cretaceous volcanic rocks were common in the study area, which have the alteration products of smectite (Fig. S4a,o), corrensite and/or chlorite-smectite (Fig. S4b,g,i) and illite-smectite (Fig. S4s). See Table S1 and Demir (2021) for the respective locations of the regional basement rock sampling.

Evaluation of the clays for industrial applications

Although this study focuses on the climatic and tectonic implications of the clay chemical and mineral trends, we also consider pragmatic aspects of their properties regarding the industrial importance of these clay deposits. The Şile clay region began to undergo significant mining in 1980, at which time refractory clays were exploited for the ceramics sector. Mining companies producing clays today include Gözde Eren & Erel, Matel, Toprak Seramik, Bilek Madencilik, Etiler Madencilik, Daşdan Madencilik, Esan, Eryılmazlar, Er Madencilik, Ergören, Ertepe, Alyans, Sörhaz, Söğüter and Mitaş. In recent years, total clay production in the region was ~2.5 million tons (MT) per year (Genç, 2019). Annual clay production for 2021 reached 3.7 MT. Most of the production (~85%) is used for the domestic market, where the Şile region supplies 90% of the clay used for ceramic square tiles, for example. The Şile clays are also used as ball clays, fire clays and, in limited cases, high-iron refractory clays, where, in addition to the square floor tile market, other products include porcelain and vitrified ceramics for the health and technical industries. Clay-producing companies consider LOI, Al_2O_3, Fe_2O_3, SiO_2 and organic matter content in their quality evaluations. Also considered are shrinkage, water adsorption, colour and strength properties. The quartz-rich sand that often caps the clay deposits are also mined and used for filling, casting, filter materials and in the building industry throughout the area, including in the İstanbul, Thrace and Marmara regions. The sands are variable in size and composition, with the whiter, homogeneous, quartz-rich sands having higher value. The total quartz sand export from the region over the past 20 years is ~20 MT. Total sand production in 2018 was 4.5 MT (Genç, 2019).

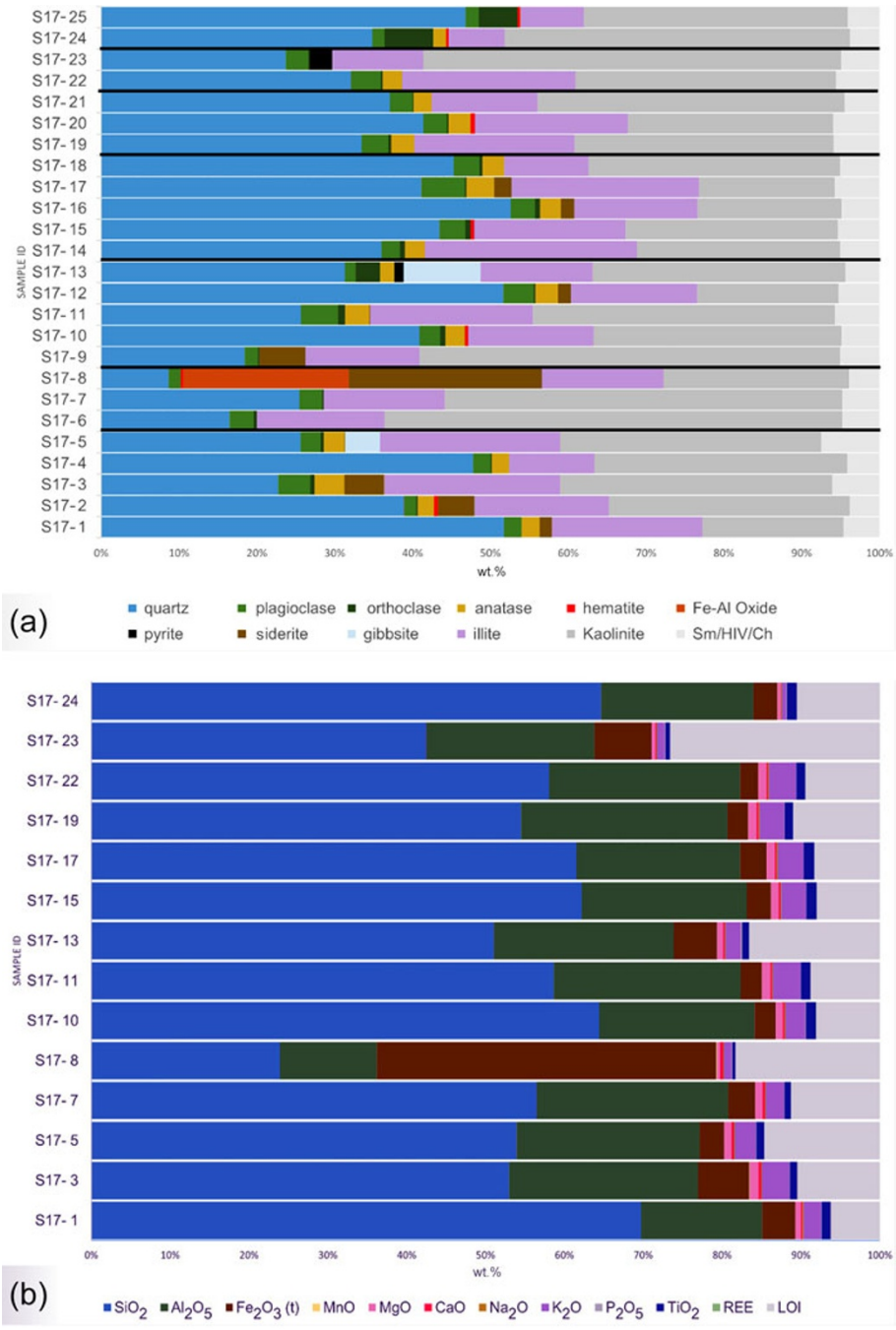

Figure 3. (a) Quantitative XRD analysis (wt.%) for the stratigraphic section of the Erel Maden mine. (b) Major oxide (wt.%) for the stratigraphic section of the Erel Maden mine. Sample numbers correspond with those given in Figure. 2. See Table S2 for all elemental data. Ch = chlorite; HIV = hydroxy-interlayered vermiculite; REE = rare earth elements; Sm = smectite.

The suitability of Şile clay for porcelain tile production is not only dependent on the composition of the raw ore from the mines but also on the fluxes and the degree of pre-milling (Yavuz *et al.*, 2011; Aras, 2018). Yavuz *et al.* (2011) noted that various combinations of clays and fluxes led to optimal plasticity, green strength and colour of the fired products. A formulation of 1:1 plastic kaolinite-rich clays and non-plastic albite, K-feldspar and quartz represents a high-quality combination (depending on the application). Sintering at fast firing rates (1200°C over 50 min) creates a product bearing residual quartz, feldspar, newly formed mullite and a glass matrix. The main underclays in the Şile region and in the Agacli-Kemerburgaz region (to the west of the Bosphorus) provide an abundant and valuable resource for making porcelain, tile, sanitary and tableware products. Yavuz *et al.* (2011) examined the firing properties of Şile clay (1212°C over 34 min) and observed 6.45% shrinkage, 3.5% water absorption, 4.10 N mm^{-2} breaking strength and chromatic values of $L^*a^*b^*$ of 69.28, 7.06 and 24.24, respectively. This same material had a chemical composition of SiO_2 (60.8%), Al_2O_3 (23.8%), Fe_2O_3 (2.5%), TiO_2 (1.2%), CaO (0.1%), MgO (0.4%), Na_2O (0.0%; not detected), K_2O (2.3%) and LOI (8.9%). Yavuz *et al.* (2011) further noted that water absorption and flexural strength are the most important properties for ceramic products used in civil construction. Water absorption is related to porosity, which is lost upon sintering above 900°C. From 900°C to 1200°C, the flexural strength increases significantly from ~30 to 150 kg cm^{-2}. The L^* (lightness value) also tends to decrease with

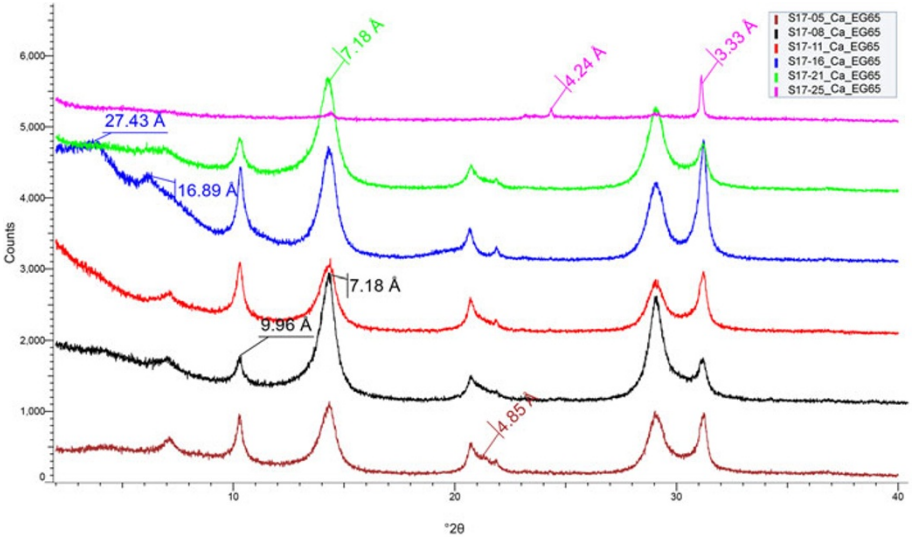

Figure 4. Representative orientated XRD traces of the <2 μm fraction (Mg- and EG-saturated) showing clay minerals present in the stratigraphic section of the Erel Maden mine. Labels mark major reflections correspond to the following minerals: quartz (4.24 and 3.33 Å), kaolinite (7.18 Å), illite (9.96 Å), gibbsite (4.85 Å) and ordered illite-smectite (27.43 and 16.89 Å). Sample numbers correspond with those given in Figure. 2. Data collected using Co-$K\alpha$ radiation.

increasing peak firing temperature (L^* is calculated using the cube root of relative luminance offset to near-black, or, more simply, $L^* = 0$ = black and $L^* = 100$ = white).

It has been noted since Roman times that adding 10% fine calcite improves the physical properties of ceramics for a wide range of uses (Schmidt-Reinholz & Schmidt, 1997). Aras (2018) performed interesting experiments using Şile clay to explore the roles of alkaline- and alkaline-earth-flux effects on the phases formed in ceramics. Additions of K- and Na-fluxes resulted in eutectic melts, whereas Ca- and Mg-fluxed forms resulted in solid-state reactions (Aras, 2004). With lower alkaline-earth content, there is a tendency towards the formation of glass phases, but the presence of Mg inhibits melt formation and changes the phase assemblages towards feldspar formation. Çelik (2010) investigated a clay sample from the Şile region for its application in the ceramic industry and noted that the Şile clays (i.e. IC) are more illite-rich clays than the clays from Afyon Province in central Anatolia, Türkiye (i.e. AC). Both the IC and AC in the study of Çelik (2010) contained montmorillonite, whereas the clays in this study did not. Çelik's (2010) measurement of the plasticity and liquid limits for the IC and AC revealed that the IC had a lower plasticity limit and a higher liquid limit than the AC. We would expect the Şile clays in our study with the highest illite to kaolinite ratios to have greater plasticity and liquid limits (higher than the IC and AC). This is supported by statements from the quarry operators describing the zones from which come the clays of highest quality that are most preferred by their clients in the ceramic industry (see also Fig. S5).

Evaluation of the clays regarding the geological evolution of Şile region

Beyond the interest in the use of Şile clays in industry, the clays' mineral and chemical properties have been used to support a prevailing hypothesis that these clay-rich accumulations formed in Neogene lacustrine basins, primarily derived from the alteration products of volcanic rocks in the surrounding region during a period of intense chemical weathering (Yeniyol, 1984; Çoban *et al.*, 2002; Ece & Nakagawa, 2003; Ece *et al.*, 2003). However, questions remain regarding what other geological factors might have influenced their genesis, including: (1) the potential involvement of other source rocks in addition to volcanic rocks; and (2) the role of recent, millennia-scale alteration due to meteoric (i.e. CZ) processes.

A conceptual model is proposed herein that incorporates both the multiple sources contributing to the formation of the Şile clay deposits and the influence of recent terrestrial weathering. Preliminary mineralogical data from nearby weathered Mesozoic outcrops, collected in 2019, provide key evidence to support this hypothesis. Additional mineral and chemical data from other Miocene clay mines in the region (Demir, 2021) further improve our understanding. A more comprehensive study to test these ideas, including a broader regional synthesis, is posited by Demir (2021). Nonetheless, the introduction of a multiple-source model for the genesis and evolution of the Şile clay deposits is a significant step forwards in understanding their formation.

Ece *et al.* (2003) proposed a two-stage model for the origin of the Şile clay deposits. The first stage involved the intense chemical weathering of andesitic rocks, tuffs and ashes at the base of the lacustrine basin. The second stage saw the erosion of andesitic rocks from the surrounding area, which were transported to the delta–swamp environment, ultimately producing kaolinite-rich formations. These kaolinite-rich formations were found to contain up to 10 m of red and brown palaeosols at their lowermost levels (Emre *et al.*, 2021), which are probably the equivalent of highly weathered volcanogenic saprolites, such as those observed in the present-day weathering volcano-sedimentary rocks examined in this study.

Evidence from modern weathering processes in nearby outcrops supports the notion that the Şile clay deposits originated from volcanic rocks. For instance, alteration products such as illite, mixed-layer chlorite-smectite (corrensite) and kaolinite were found in both surface outcrops of andesite and in nearby drill cores (Demir, 2021). In contrast, examination of fresher outcrops of andesite-bearing albite and calcite revealed corrensite but no kaolinite or discrete smectite, lending further support to the conclusion that the Şile clays were indeed sourced from volcanic materials. It is suggested that the corrensite is a product of hydrothermal alteration of the volcanics.

Beyond volcanic rocks, this study also considers the possible influence of other basement rock types on the composition of the

Şile clay deposits. Examination of the mineralogy of Cretaceous flysch basement rocks revealed a mineral assemblage resembling that of andesitic rocks, along with additional minerals such as chlinochlore, $2M_1$ muscovite and laumontite, which suggest low-grade hydrothermal alteration. The weathered Cretaceous basalts, as described by Yavuz & Yilmaz (2010), revealed significant amounts of discrete smectite in the weathered fine-grain fraction, alongside other minerals typical of mafic volcanic assemblages (e.g. albite, hornblende, augite, chlorite, opal, sanidine and illite). These findings support the idea that other basement rocks, in addition to volcanic materials, may have slightly contributed to the provenance of the Miocene lacustrine sediments.

Once deposited, the presence of siderite and pyrite in the lower sections of the Şile clays suggests that bicarbonate-rich conditions were present during the early diagenesis of the lacustrine sediments. In addition to bicarbonate produced by sulfate reduction, additional bicarbonate contributions may be derived from the weathering of nearby Mesozoic limestones. While detrital and authigenic calcite were not observed in the Şile clay deposits in this study, the siderite distribution implies that a source of bicarbonate existed, which could be linked to the diagenetic environment that was reducing with limited amounts of sulfide. What sulfide was present in the system was probably sequestered into the pyrite that is found in minor amounts.

An important aspect of this study is the recognition of the role of recent weathering processes in shaping the mineralogy of the Şile clay deposits. Using the CIA (Nesbitt & Young, 1982), it was observed that the sand layers above the clay deposits exhibited very high CIA values (>93), indicating significant modification by meteoric weathering. All clay samples within the deposit showed CIA values >83, reflecting a history of moderate to intense weathering. Notably, slightly higher CIA values and gibbsite were found directly below each coal seam compared to farther below, suggesting that organic acids derived from the coal have driven hydrolysis reactions, influencing mineral alteration. This underscores the importance of organic acids and their role in weathering processes within the CZ. Added to this is the slight trend of less negative (–93 to –70) CMAI values proceeding upwards across the entire section, as highly negative CMAI values are indicators of an intense chemical weathering environment promoted by a wet and warm climate with tectonic uplift, promoting the flushing of weathering reactants (Schroeder, 2018).

The distribution of ferrous minerals such as pyrite and siderite and ferric minerals such as goethite provide further evidence of CZ weathering. The oxidation of these ferrous minerals to form ferric minerals is associated with the presence of meteoric waters. Ferric minerals were observed in the lower sections of the deposit and were absent from the uppermost levels of the clay sequence, except for the vertical clay dike cross-cutting the capping sand section. The formation of ferric oxidation bands and the reddish staining at various levels of the mine suggest that CZ weathering is not simply a top-down process. Instead, it appears to propagate laterally, influenced by proximity to coal seams. Organic matter, which is known to serve as an electron donor, may facilitate this process by influencing the oxidation of ferrous minerals from the bottom up or laterally, as described by Schroeder *et al.* (2004).

The geological evolution of the Şile clay deposits involves multiple contributing factors, primarily including volcanic rock weathering, with contributions from other basement rock types, and recent alteration by meteoric weathering in the CZ. This study introduces these factors to the conceptual model, thus providing a more comprehensive understanding of the genesis of the Şile clay deposits. The complex interactions between geological processes, including sedimentation, weathering and diagenesis, have shaped the mineralogy and composition of the clay deposits, which in turn have implications for both their geological history and their industrial applications. Further regional studies of other clay deposits are needed to refine and expand this model for the formation and alteration of the Şile clay deposits.

Independent palynoflora studies (Kayseri-Özer, 2013) and numerous other studies demonstrate that western Anatolia experienced a warm palaeoclimate, with abundances of swamps and grassland species. The same studies suggest that the Burdigalian–Langhian interval (~20–16 Ma; i.e. prior to deposition of the Şile clays) was the warmest in the region during the Miocene, followed by a period of cooling. The appearance of mesothermic forests, which would coincide with cooling temperatures (associated with higher elevations), is also suggested by the regional palynofloras. Inferred mean annual precipitation and temperature from north Germany were posited to decrease from ~1400 to 1100 mm and from ~17°C to 13°C during the latter part of the Miocene (Zachos *et al.*, 2001). It is therefore suggested that the Şile clay deposits were influenced by the changing climate (cooler and dryer), with oscillatory influences during weathering and deposition. The coincidental onset of the North Anatolian Fault from ~13 to 11 Ma propagating westwards is a sufficient mechanism for creating shear-related deformation over a broad region, with recent evidence for this process being the observed cyclical seismic behaviour (Şengör *et al.*, 2005).

Combining the mineral and chemical data from this study with previous studies, including those from the similar deposits and palaeontological analyses, supports the hypothesis that the properties of the Şile clays have been influenced by numerous geological factors. Intense chemical weathering of Cretaceous andesites resulted in sediments with highly negative CMAI values and high CIA values. Analysis of modern chemical weathering in other regional parent rocks, including flysch, carbonates and basalts, indicates that these may also have served as minor provenance sources for the lacustrine deposits.

Cyclically deposited organic-rich sediments (now coals) locally modified underclays during diagenesis. The repeating fining-upwards cycles of sediment, with an overall trend towards less negative CMAI values, indicate a decrease in chemical weathering intensity, consistent with a cooling climate. The cyclic nature of deposition may also have been influenced by periodic uplift associated with the initiation of the North Anatolian Fault (~13–11 Ma). Since that time, further deposition may have occurred, but subsequent erosion associated with continued uplift has exposed the clay deposits near the present-day surface.

Finally, the apparent oxidation front, indicated by the absence of ferrous minerals (siderite and pyrite) in the upper sections of the clay deposit, suggests that recent CZ processes are actively modifying the mineral and chemical properties in the near surface to depths of tens of metres. This does not discount the influence of redox transition produced during diagenesis. We suggest that a ^{14}C study of the carbon included in the goethite and/or gibbsite would offer evidence for formation due to modern oxidation (Schroeder *et al.*, 2001; Yapp, 2001).

Conclusions

The analysis of clay samples from the actively mined deposit in Şile, Türkiye, reveals a diverse mineral assemblage dominated by kaolinite and illite, with smaller amounts of interstratified

chlorite-smectite, discrete chlorite, vermiculite, gibbsite and goethite. These findings highlight the complex mineralogical composition of the lacustrine sediments and suggest that their deposition occurred in a dynamic environment influenced by tectonic uplift associated with the North Anatolian Fault and climatic oscillations. The presence of cyclothem-like sequences, each marked by thin coal seams, further supports the hypothesis of episodic deposition driven by fluctuating environmental conditions.

This study underscores the potential utility of sections with higher illite-to-kaolinite ratios in the ceramics industry, as these deposits exhibit favourable plasticity and liquid limits, making them well-suited for industrial applications. The mineralogical distinction between weathered and less weathered clays can help guide future exploration and exploitation of Şile's clay resources. Moreover, the comparison of mineral assemblages between the Şile clay deposits and nearby weathered basement rocks suggests that weathered Cretaceous andesites played a significant role in sediment sourcing while also hinting at possible contributions from Palaeozoic meta-sediments and limestones during the Miocene.

The observed distribution of accessory minerals such as pyrite and siderite indicates that dysoxic conditions prevailed during deposition and diagenesis, reflecting a unique depositional environment. The oxidation of pyrite and siderite and the subsequent formation of iron oxide minerals, including goethite, highlight the ongoing impacts of meteoric weathering processes on the clay deposits over the past millennia. These findings suggest that CZ processes have extended deeper into the subsurface than previously anticipated, with meteorological influences continuing to reshape the mineralogy of the Şile clay deposits.

Supplementary material. The supplementary material for this article can be found at https://doi.org/10.1180/clm.2025.10009.

Acknowledgements. The authors appreciate access to the ERAL MADEN Şile mining sites provided by Cafer.

Financial support. The authors were aided by support to HD from the UGA Department of Geology and to PAS from the TUBITAK Eminent Visiting Scholar Fellowship.

Competing interests. The authors declare none.

References

Adamia S.A., Gamkrelidze I.P., Zakariadze G.S. & Lordkipanidze M.B. (1974) Adjaro-Trialetsky progib I problema formirovaniya glubokovodnoi vpadiny Chernoga moray. *Geotektonika* **1**, 78–94.

Şengör A.M.C & Kindap T. (2019) The geology and geomorphology of İstanbul. Pp. 249–263 in: *Landscapes and Landforms of Turkey* (C. Kuzucuoğlu, A. Çiner & N. Kazancı, editors). Springer, Berlin, Germany.

Aras A. (2004) The change of phase composition in kaolinite- and illite-rich clay-based ceramic bodies. *Applied Clay Science*, **24**, 257–269.

Aras A. (2018) The differences between alkaline- and alkaline-earth-flux effects on high-temperature phase change of clay based ceramic. *Applied Clay Science*, **164**, 2–12.

Austin J.C., Richter D.D. & Schroeder P.A. (2020) Quantification of mixed-layer clays in multiple saturation states using NEWMOD2: implications for the potassium uplift hypothesis in the SE United States. *Clays and Clay Minerals*, **68**, 67–80.

Awwad A.M., Amer M.W. & Al-Aqarbeh M.M. (2020) TiO_2-kaolinite nanocomposite prepared from the Jordanian kaolin clay: adsorption and thermodynamics of Pb(II) and Cd(II) ions in aqueous solution. *Chemistry International*, **6**, 168–178.

Aysal N., Keskin M., Peytcheva I. & Duru O. (2018) Geochronology, geochemistry and isotope systematics of a mafic–intermediate dyke complex in the İstanbul Zone. New constraints on the evolution of the Black Sea in NW Turkey. *Geological Society, London, Special Publications*, **464**, 131–168.

Bozkurt E. (2001) Neotectonics of Turkey – a synthesis. *Geodynamica Acta*, **14**, 3–30.

Cao Z., Yuefa J., Qizhao W. & Cheng, H. (2021) High-efficiency photo-Fenton Fe/g-C_3N_4/kaolinite catalyst for tetracycline hydrochloride degradation. *Applied Clay Science*, **212**, 106213.

Çelik H. (2010) Technological characterization and industrial application of two Turkish clays for the ceramic industry. *Applied Clay Science*, **50**, 245–254.

Churchman G.J. (1990) Relevance of different intercalation tests for distinguishing halloysite from kaolinite in soils. *Clays and Clay Minerals*, **38**, 591–599.

Çoban F., Ece Ö.I, Yavuz O. & Özdamar Ş. (2002) Petrogenesis of volcanic rocks, and clay mineralogy and genesis of underclays, Şile region, İstanbul. *Neues Jahrbuch für Mineralogie*, **178**, 1–25.

Demir H. (2021) *A New Look at Şile Clay Deposits, Eastern İstanbul: Detailed Characterization and Provenance*. MSc thesis. University of Georgia. Retrieved from https://esploro.libs.uga.edu/esploro/outputs/graduate/A-NEW-LOOK-AT-ŞILE-CLAY/9949375150102959#file-0

Dong X., Richter D.D., Thompson A. & Wang J. (2023) The primacy of temporal dynamics in driving spatial self-organization of soil iron redox patterns. *Proceeding of the National Academy of Sciences of the United States of America*, **20**, e2313487120.

Ece Ö.I., Nakagawa Z. & Schroeder P.A. (2003) Alteration of volcanic rocks and genesis of kaolin deposits in the Şile region northern İstanbul, Turkey. I: clay mineralogy. *Clays and Clay Minerals*, **51**, 675–688.

Fackrell L.E., Schroeder P.A., Demir H. & Rotz R.R. (2020) A critical zone approach to the study of Mars. Planetary Science and Astrobiology Decadal Survey White Paper. Lunar and Planetary Institute. Retrieved from https://www.nationalacademies.org/our-work/planetary-science-and-astrobiology-decadal-survey-2023-2032

Fellah M., Hezil N., Guerfi K., Djellabi R., Montagne A., Iost A. & Obrosov A. (2021) Mechanistic pathways of cationic and anionic surfactants sorption by kaolinite in water. *Environmental Science and Pollution Research*, **28**, 7307–7321.

Gedik İ., Pehlivan Ş., Timur E., Duru A.İ., Akbaş B., Özcan İ. & Alan İ. (2005) Kocaeli *Yarımadası'nın Jeolojisi* [*Geology of Kocaeli Peninsula*]. Mineral Research and Exploration Institute (MTA) of Turkey Report no. 10774. [in Turkish, unpublished]

Gianni E., Avgoustakis K. & Papoulis D. (2020) Kaolinite group minerals: applications in cancer diagnosis and treatment. *European Journal of Pharmaceutics and Biopharmaceutics*, **154**, 359–376.

Görür N. (1988) Timing of opening of the Black Sea basin. *Tectonophysics*, **147**, 247–262.

Görür N. (1991) Aptian–Albian palaeography of Neotethyan domain. *Palaeogeography, Palaeoecology*, **87**, 267–288.

Görür N. (1997) Cretaceous syn- to post-rift sedimentation on the southern continental margin of the western Black Sea basin. Pp. 227-240 in: *Regional and Petroleum Geology of the Black Sea and Surrounding Region* (A.G. Robinson, editor). American Association of Petroleum Geologists, Memoirs, 68. American Association of Petroleum Geologists, Tulsa, OK, USA.

Hsü K.J., Nacev I.K. & Vuchev V.T. (1977) Geologic evolution of Bulgaria in the light of plate tectonics. *Tectonophysics*, **40**, 245–256.

Kayseri-Özer M.S. (2013) Spatial distribution of climatic conditions from the Middle Eocene to Late Miocene based on palynoflora in central, eastern and western Anatolia. *Geodinamica Acta*, **26**, 122–157.

Ketin İ. (1955) Yozgat bölgesinin jeolojisi ve Orta Anadolu masifinin tektonik durumu. *Türkiye Jeoloji Bülteni*, **6**, 1–40.

Ketin İ. (1966) Anadolu'nun Tektonik Birlikleri. *Mineral Research and Exploration Institute of Türkiye (MTA) Bulletin*, **66**, 20–34. [In Turkish with English abstract]

Le Pichon X., Şengör A.M.C & Demirbağ E. (2001) The active main Marmara fault. *Earth and Planetary Science Letters*, **192**, 595–616.

Letouzey J., Biju-Duval B., Dorkel A., Gonnard R., Kristchev K., Montadert L. & Sungurlu O. (1977) The Black Sea: a marginal basin; geophysical and

geological data. Pp. 363–376 in: *International Symposium on the Structural History of the Mediterranean Basins* (B. Biju-Duval & L. Montadert, editors). Editions Technip, Paris, France.

Lom N., Ülgen S.C., Sakınç M. & Şengör A.M.C. (2016) Geology and stratigraphy of Istanbul region. *Geodiversitas*, **38**, 175–195.

Manetti P., Boccaletti M. & Peccerillo A. (1988) The Black-Sea: remnant of a marginal basin behind the Srednogorie–Pontides island arc system during Upper Cretaceous–Eocene time. *Bolletino di Geofisica Teorica ed Applicata*, **30**, 39–51.

Mubarak M.F., Shehata N. & Ahmed H.A. (2021) Adsorption mechanism for mitigation of toxic Zn^{2+} from synthetic polluted water onto blended composite of chitosan/kaolinite. *Journal of Chemical Technology & Metallurgy*, **56**, 133–144.

Murray H.H. & Keller W.D. (1993) Kaolins, kaolins, and kaolins. In: *Kaolin Genesis and Utilization* (H.H. Murray, W.M. Bundy & C.C. Harvey, editors). Clay Minerals Society Special Publications. Retrieved from https://doi.org/10.1346/CMS-SP-1.1

Nesbitt H.W. & Young G.M. (1982) Early Proterozoic climates and plate motions inferred from major element chemistry of lutites. *Nature*, **299**, 715–717.

Emre Ö., Kondo K., Özalp S. & Elmacı H. (2021) Fault geometry, segmentation and slip distribution associated with the 1939 Erzincan earthquake rupture along the North Anatolian Fault, Turkey. *Geological Society*, *London*, *Special Publications*, **501**, 23–70.

Okay A.I. (1989) Tectonic units and sutures in the Pontides, northern Türkiye. Pp. 109–116 in: *Tectonic Evolution of the Tethyan Region* (A.M.C. Şengör, editor). Kluwer Academic Publishers, Dordrecht, The Netherlands.

Okay A.I., Bozkurt E., Satır M, Yiğitbaş E, Crowley Q.G. & Shang C.K. (2008) Defining the southern margin of Avalonia in the Pontides: geochronological data from the Late Proterozoic data from Ordovician granitoids from NW Turkey. *Tectonophysics*, **461**, 252–264.

Okay A.I. & Kelley S.P. (1994) Tectonic setting, petrology and geochronology of jadeite + glaucophane and chloritoid + glaucophane schists from north-west Turkey. *Journal of Metamorphic Geology*, **12**, 455–466.

Okay A.I., Tüysüz O., Satır M., Ozkan-Altiner S., Altiner D., Sherlock S. & Eren R.H. (2006) Cretaceous and Triassic subduction-accretion, high-pressure–low-temperature metamorphism, and continental growth in the Central Pontides, Turkey. *Geological Society of America Bulletin*, **118**, 1247–1269.

Olu-Owolabi B.I., Diagboya P.N., Mtunzi F.M. & Düring R.A. (2021) Utilizing eco-friendly kaolinite–biochar composite adsorbent for removal of ivermectin in aqueous media. *Journal of Environmental Management*, **279**, 111619.

Özgül N. (2011) *İstanbul İl Alanının Jeolojisi*. İstanbul Büyükşehir Belediyesi, Planlama ve İmar Daire Başkanlığı Zemin ve Deprem İnceleme Müdürlüğü, İstanbul, Türkiye, ix + 89 pp.

Özgül N. (2012) Stratigraphy and some structural features of the Istanbul Paleozoic. *Turkish Jounal of Earth Sciences*, **21**, 817–866.

Rashad Y.M., El-Sharkawy H.H., El-Kenawy M.A. & Galilah D.A. (2023) Kaolin triggers defense-responsive genes in grapevines (cv. King Ruby seedless) to downy mildew and enhances its vegetative development, production, and berries quality standards. *Scientia Horticulturae*, **309**, 111674.

Richter D.D., Eppes M.C., Austin J.C., Bacon A.R., Billings S.A., Brecheisen Z. *et al.* (2020) Soil production and the soil geomorphology legacy of Grove Karl Gilbert. *Soil Science Society of America Journal*, **84**, 1–20.

Rietveld H.M. (1967) Line profiles of neutron powder-diffraction peaks for structure refinement. *Acta Crystallographica*, **22**, 151–152.

Genç Ş.C. (2019) *Şile Bölgesi kil ve kumlarının başta seramik sektörü olmak üzere ilgili diğer sektörler için ekonomik öneminin ortaya konulması* [*Revealing the Economic Importance of Clay and Sands in the Şile Region, Especially for the Ceramics Industry and Other Related Sectors*]. Technical report prepared on behalf of the Seramik Araştırma Merkezi. İstanbul Technical University, İstanbul, Türkiye.

Schmidt-Reinholz C. & Schmidt H. (1997) The effect of lime and dolomite in brick bodies and finished products – part 1. *Tile & Brick International*, **13**, 14–16.

Schroeder P.A. (2018) *Clays in the Critical Zone*. Cambridge University Press, Cambridge, UK, 252 pp.

Schroeder P.A., Melear N.D., Bierman P., Kashgarian M. & Caffee M.W. (2001) Apparent gibbsite growth ages for regolith in the Georgia Piedmont. *Geochimica et Cosmochimica Acta*, **65**, 381–386.

Schroeder, P.A., Pruett, R.R. & Melear N.D. (2004) Crystal-chemical changes in an oxidative weathering front in a middle Georgia kaolin deposit. *Clays and Clay Minerals*, **52**, 212–220.

Şengör A.M.C., Görür N. & Şaroğlu F. (1985) Strike-slip faulting and related basin formation in zones of tectonic escape: Türkiye as a case study: *SEPM Special Publication*, **37**, 227–264.

Şengör A.M.C., Tüysüz O., İmren C., Sakınç M., Eyidoğan H., Görür N. *et al.* (2005) The North Anatolian Fault: a new look. *Annual Review of Earth and Planetary Science*, **33**, 37–112.

Şengör A.M.C. & Yilmaz Y. (1981) Tethyan evolution of Turkey: a plate tectonic approach. *Tectonophysics*, **75**, 181–241.

Toby B.H. (2006) *R* factors in Rietveld analysis: how good is good enough? *Powder Diffraction*, **21**, 67–70.

Wanless H.R. & Weller J.M. (1932) Correlation and extent of Pennsylvanian cyclothems. *GSA Bulletin*, **43**, 1003–1016.

Warr L.N. (2022) Earth's clay mineral inventory and its climate interaction; a quantitative assessment. *Earth-Science Reviews*, **234**, 104198.

Yapp C.J. (2001) Mixing of CO_2 in surficial environments as recorded by the concentration and $\delta^{13}C$ values of the $Fe(CO_3)$ OH component in goethite. *Geochimica et Cosmochimica Acta*, **65**, 4115–4130.

Yavuz O., Kayaci K., Kucuker A.S., Ozdamar S., Uzun M., Yanik G. *et al.* (2011) Characterization of underclays from Agacli-Kemerburgaz region of İstanbul/Türkiye and their evaluation for porcelain tile production. *Industrial Ceramics*, **31**, 183–191.

Yavuz O. & Yilmaz Y. (2010) İstanbul kuzeyi volkanitlerinin jeolojik, petrografik ve mineralojik özellikleri. *ITU Journal Series D: Engineering*, **9**, 38–46.

Yeniyol M. (1984) İstanbul killerinin oluşumu. *Türkiye Jeoloji Kurultayı Bülteni*, **5**, 143–150.

Yılmaz Y. (1993) New evidence and model on the evolution of the southeast Anatolian orogen. *GSA Bulletin*, **105**, 251–271.

Yurtsever A. (1982) *Kocaeli Triyası biyostratigrafi projesi, Gebze-Hereke-Tepecik alanında Mesozoyik kayalarının jeolojisi*. MTA Report no. 7195. Turkish General Directorate of Mineral Research and Exploration, Ankara, Türkiye.

Zachos J., Pagani M., Sloan L., Thomas E. & Billups K. (2001) Trends, rhythms, and aberrations in global climate 65 Ma to present. *Science*, **292**, 686–693.

Zhang B., Guo H., Deng L., Fan W., Yu T. & Wang Q. (2020) Undehydrated kaolinite as materials for the preparation of geopolymer through phosphoric acid-activation. *Applied Clay Science*, **199**, 105887.

Zunino F., Boehm-Courjault E. & Scrivener K. (2020) The impact of calcite impurities in clays containing kaolinite on their reactivity in cement after calcination. *Materials and Structures*, **53**, 44.